Modal and nonmodal growths of inviscid planar perturbations in shear flows with a free surface

Nikolaos A. Bakas[a] and Petros J. Ioannou
Department of Physics, National and Kapodistrian University of Athens, Zografos 15784, Greece

(Received 30 June 2008; accepted 4 December 2008; published online 4 February 2009)

Shear flows with a free surface possess diverse branches of modal instabilities. By approximating the mean flow with a piecewise linear profile, an understanding and classification of the instabilities can be achieved by studying the interaction of the edge waves that arise at the density discontinuity at the surface and the vorticity waves that are supported at the mean vorticity gradient discontinuities in the interior. The various branches of instability are identified and their physical origin is clarified. The edge waves giving rise to the modal instabilities can also lead to a modest transient growth that extends into the regions of neutrality of the flow. However, when the continuous spectrum is excited substantial transient growth can arise and the optimal perturbations attain greater energy when compared with the energy of the fastest modal growing perturbation. These optimal perturbations utilize the continuous spectrum to excite at large amplitude the neutral or amplifying modes of the system. © *2009 American Institute of Physics*.
[DOI: 10.1063/1.3072617]

I. INTRODUCTION

Stability of shear flows with an upper free surface is of interest both in geophysics and in engineering. Such flows arise at the crest of a spilling breaker,[1,2] in viscous ship wakes,[3] in wind-drift currents at the ocean surface developing over large horizontal distances and breaking into turbulent mixing layers,[4] and in high speed liquid jets[5] used for designing liquid-metal forced flow targets and fusion reactor liquid wall/blankets.

Previous studies of surface shearing currents considered a surface layer of uniform vorticity overlying a stationary layer of infinite depth[4,6,7] and showed that the flow is unstable for a limited range of zonal wavenumbers. Triantafyllou and Dimas[3] computed the linear stability of the shear flow observed in experiments of wakes behind a hydrofoil and found two kinds of normal mode instabilities: branch I, which exists for low wavenumbers and resembles the varicose mode in an infinite flow, and branch II, which exists for higher wavenumbers and resembles the unstable modes found by Stern and Adam.[4] In order to understand the instabilities found by Triantafyllou and Dimas,[3] Longuet-Higgins[8] approximated the shear layer with a piecewise linear velocity profile, reducing the stability problem to the study of the roots of a quartic polynomial. Although the stability regimes obtained by Longuet-Higgins[8] did not numerically correspond to those of the original smooth profile,[9] the piecewise linear profile analysis possessed the same instability branches and revealed the relation between the branches in a transparent way. We will use this simplified flow in the present study as well.

The goal of this study is to gain further insight into the perturbation growth mechanisms by first rationalizing the modal instabilities in terms of the interaction between vorticity and gravity edge waves at the interfaces of vorticity and density discontinuities and then by addressing the nonmodal interaction of the edge waves, as well as assessing the role of the continuous spectrum in perturbation growth.

Interaction between vorticity edge waves was pioneered by Bretherton[10] to explain baroclinic instability and cyclone growth in the atmosphere. Bretherton[10] showed that the instability is understood in terms of a constructive interaction between two counterpropagating Rossby waves located in regions of opposite signs of mean potential vorticity gradient. The waves interact by inducing velocity that advects the mean potential vorticity in the region of the opposed wave, and depending on their phase difference, they can modify the zonal propagation rate of the other Rossby wave and can also change its amplitude. Bretherton[10] concluded that normal mode instability occurs when these two waves resonate, that is, when their phases lock and propagate with the same phase speed in a growing configuration. Harnik and Heifetz[11] discussed in a similar manner barotropic instability of shear flows and Heifetz *et al.*[12] discussed shear instability of a constant shear flow embedded between constant flows as was modeled by Rayleigh.[13]

On the other hand, Taylor[14] and Goldstein[15] recognized that shear instability in a fluid with layers of different densities can be regarded as the resonance of edge waves at the interfaces of density discontinuity. Recent studies extended Taylor's analysis to include interaction between edge waves on vorticity and density discontinuities and were able to explain Kelvin–Rossby wave instabilities in a shallow water model[16] and the classic Holmboe instability.[17]

Although theoretical interest in terms of edge wave interactions was mainly focused on understanding modal perturbation growth, Heifetz and Methven[18] demonstrated that

[a]Author to whom correspondence should be addressed. Present address: Building IV Office 32, Panepistimiopolis, Zografos, Athens, Greece. Electronic mail: nbakas@post.harvard.edu.

the edge wave interactions not only generate the unstable discrete spectrum of the operator governing the stability of perturbations but can also produce nonmodal transient growth even for zonal wavenumbers for which exponentially growing solutions are absent. However, in addition to the discrete spectrum, shear flows also support a continuous spectrum of neutrally stable singular modes.[19–21] Even though the continuous spectrum cannot support exponential growth, it can lead to rapidly growing perturbations at finite time and needs to be included to assess the stability properties of the flow at finite time.[22,23]

In this study we investigate the stability of the shear layer with the free surface considered by Longuet-Higgins[8] using the methods of generalized stability theory.[23] We start by following Heifetz and Methven[18] and study the interaction between edge waves propagating at the levels of vorticity gradient and density discontinuities in order to obtain the exponentially growing normal modes found by Longuet-Higgins[8] and investigate the transient perturbation growth produced by the edge waves. We also determine the optimal planar perturbations, which are the most energetic structures that can arise, taking into account both the discrete (edge waves) and the continuous spectrum and examine the role of a continuous spectrum in optimal growth. The transient growth associated with three dimensional perturbations will be the subject of future work.

This paper is organized as follows. In Sec. II we describe the linear evolution equations for perturbations in a horizontal shear flow with a free surface and interpret the emerging instabilities in terms of the interactions between vorticity and gravity waves propagating at the interfaces of vorticity gradient and density discontinuities. Section III describes the temporal development of the edge waves leading to transient growth of perturbation energy and the role of continuous spectrum in nonmodal growth. We finally end with a brief discussion and our conclusions in Sec. IV.

II. FORMULATION OF THE STABILITY PROBLEM

We consider after Longuet-Higgins[8] a homogeneous, incompressible, and inviscid fluid of density ρ_0 in the unbounded region $y<0$, where y is the vertical coordinate. At equilibrium, $y=0$ is the free surface of the fluid, and $U(y)$, shown in Fig. 1, is the mean zonal shear flow given by

$$U(y)=\begin{cases} V_0 & \text{for} -H_1 < y \le 0, \\ V_0(y+H_2)/(H_2-H_1) & \text{for} -H_2 < y \le -H_1, \\ 0 & \text{for } y \le -H_2. \end{cases} \tag{1}$$

Zonal, u, and vertical, v, perturbation velocities varying only in the zonal, x, and vertical, y, directions are superposed on the equilibrium mean flow, while $\zeta(x,t)$ is the small elevation of the free surface, p is the pressure perturbation superposed on the mean hydrostatic pressure field, and ρ is the density perturbation superposed on the mean density ρ_0. Neglecting surface tension, the linearized, nondimensional equations governing the evolution of small perturbations are

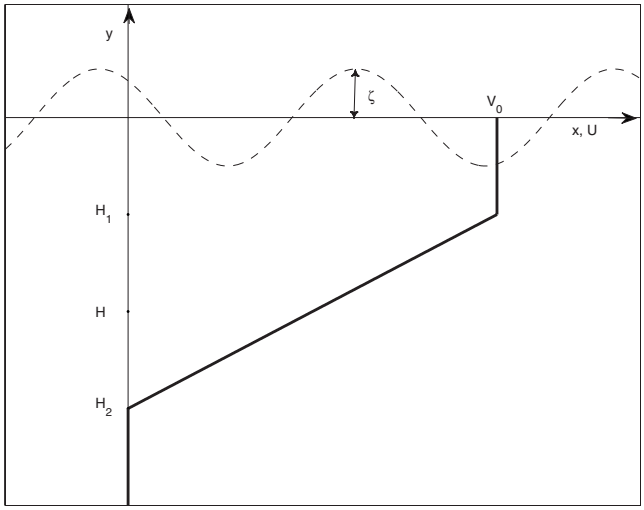

FIG. 1. Vertical velocity profile (1). The dashed line shows the displacement ζ of the free surface from the equilibrium position $y=0$.

$$[\partial_t + U(y)\partial_x]u + \frac{dU}{dy}v = -\partial_x p, \tag{2}$$

$$[\partial_t + U(y)\partial_x]v = -\partial_y p - \frac{\rho}{F^2}, \tag{3}$$

$$[\partial_t + U(y)\partial_x]\rho = -v\frac{d\rho_0}{dy} = v\,\delta(y), \tag{4}$$

$$\partial_x u + \partial_y v = 0. \tag{5}$$

The horizontal and vertical scales are nondimensionalized by $H=(H_1+H_2)/2$, velocities are nondimensionalized by the mean velocity at the surface, V_0, time has been nondimensionalized by H/V_0, and pressure and density have been nondimensionalized by $\rho_0 V_0^2$ and ρ_0, respectively. The Froude number, $F=V_0/\sqrt{gH}$, is the ratio between the mean flow velocity at the surface, V_0, and the phase speed, $\sqrt{gH}$, of propagation of a shallow surface gravity wave in a gravity field of intensity g and water of depth H. Eliminating pressure from Eqs. (2) and (3), we obtain the following equation for the meridional component of vorticity, $q=\partial_y u-\partial_x v$:

$$[\partial_t + U(y)\partial_x]q = -\frac{d^2U}{dy^2}v + \frac{1}{F^2}\partial_x\rho. \tag{6}$$

At the free surface, $y=\zeta(x,t)$, the following linearized kinematic boundary condition must be satisfied:

$$(\partial_t + \partial_x)\zeta = v(y=0,t). \tag{7}$$

Equations (4) and (7) then imply that

$$\rho = \zeta\,\delta(y). \tag{8}$$

Therefore, there are three surfaces of discontinuity in this problem: at the free surface, $y=0$, there is a density discontinuity and at depths $h_1=H_1/H$ and $h_2=H_2/H$ there are two discontinuities in the vorticity gradient of the mean velocity profile (1):

$$\frac{d^2U}{dy^2} = \alpha[\delta(y+h_2) - \delta(y+h_1)], \tag{9}$$

where $\alpha=1/(h_2-h_1)$ is the nondimensional shear. Introducing a streamfunction $\tilde{\psi}(x,y,t)$ to express the velocity fields as $[u,v]=[\partial_y,-\partial_x]\tilde{\psi}$, taking harmonic perturbations of the form $\tilde{\psi}(x,y,t)=\psi(y,t)e^{ikx}$, and using Eqs. (8) and (9), vorticity equation (6) can be expressed in terms of the Fourier amplitude ψ as

$$[\partial_t + ikU(y)](D^2-k^2)\psi = ik\alpha\psi[\delta(y+h_2) - \delta(y+h_1)] + \frac{ik}{F^2}\zeta\delta(y), \tag{10}$$

where $D^2=\partial^2/\partial y^2$.

By integrating Eq. (10) in the neighborhood of $y=0$, $y=-h_1$, and $y=-h_2$, it can be readily shown that the solution to Eq. (10) satisfies the Rayleigh equation

$$[\partial_t + ikU(y)](D^2-k^2)\psi = 0,$$

and the three conditions at each surface of discontinuity:

$$(\partial_t + ik)\zeta = -ik\psi(0,t),$$
$$(\partial_t + ik)\partial_y\psi|_{y=0} = -ik\zeta/F^2 \quad \text{at } y=0, \tag{11}$$

$$(\partial_t + ikU_1)[\partial_y\psi]_{-h_1} = -ik\alpha\psi(-h_1) \quad \text{at } y=-h_1, \tag{12}$$

$$(\partial_t + ikU_2)[\partial_y\psi]_{-h_2} = ik\alpha\psi(-h_2) \quad \text{at } y=-h_2, \tag{13}$$

where $[\cdot]_y$ denotes the discontinuity at y and $U_1=1$ and $U_2=0$ are the mean velocities at $y=-h_1$ and $y=-h_2$, respectively. The first condition in Eq. (11) is the kinematic boundary condition (7), while the second one is the dynamic boundary condition at the surface in the absence of surface tension. We also demand that the solutions decay as $y\to-\infty$.

The discrete modes of the linearized operator governing the evolution of perturbations are synthesized by superposing the three edge waves supported at each discontinuity interface. Each edge wave satisfies $(D^2-k^2)\psi=0$ in $y<0$ and only one of the three matching conditions, Eq. (11), Eq. (12), or Eq. (13).

Consider first the edge wave at the free surface $y=0$:

$$\psi_0(y,t) = \frac{1}{k}e^{ky}e^{-i(k\pm\sqrt{k}/F)t},$$

which satisfies $(D^2-k^2)\psi=0$ in $y<0$, and Eq. (11). It represents two surface gravity waves propagating with nondimensional phase speeds:

$$c_\pm = 1 \pm \frac{1}{F\sqrt{k}}, \tag{14}$$

and decaying exponentially with y.

The second and third edge waves are

$$\psi_i(y,t) = \frac{1}{2k}[e^{-k|y+h_i|} + e^{k(y-h_i)}]e^{-ik[U_i+(-1)^i(1+e^{-2kh_i})\alpha/(2k)]t},$$

where $i=1,2$. Both decay at $y=-\infty$ and each is supported at the mean vorticity gradient discontinuity at $y=-h_i$ with $i=1,2$, satisfying Eqs. (12) and (13), respectively. In order to clearly distinguish the vorticity edge wave solutions from the surface gravity waves we have also imposed $\partial_y\psi|_{y=0}=0$, so that the inner vorticity waves do not have an imprint on the vorticity at the surface. The vorticity edge waves propagate with phase speeds

$$c_i = U_i + (-1)^i\frac{\alpha(1+e^{-2kh_i})}{2k}, \tag{15}$$

where $i=1,2$. The first propagates retrograde relative to the mean flow U_1 at the upper interface of discontinuity while the second propagates prograde relative to the mean flow U_2 at the lower interface of discontinuity forming a counterpropagating pair of Rossby waves.[18]

The three edge waves interact with each other and the linear superposition

$$\psi(y,t) = -\frac{q_0(t)}{k}e^{ky} - \frac{q_1(t)}{2k}(e^{-k|y+h_1|} + e^{k(y-h_1)}) - \frac{q_2(t)}{2k}(e^{-k|y+h_2|} + e^{k(y-h_2)})$$

satisfies the perturbation equations if the complex amplitudes $[q_0(t),q_1(t),q_2(t)]$ are constrained by Eqs. (11)–(13) to evolve according to

$$\frac{d\mathbf{x}}{dt} = \mathbf{A}\mathbf{x},$$

where $\mathbf{x}=[q_0(t),\zeta(t),q_1(t),q_2(t)]^T$ is the state vector, and

$$\mathbf{A} = \begin{pmatrix} -ik & ik/F^2 & 0 & 0 \\ i & -ik & ie^{-kh_1} & ie^{-kh_2} \\ i\alpha e^{-kh_1} & 0 & -ikc_1 & i\alpha(e^{-k(h_2-h_1)}+e^{-2k})/2 \\ -i\alpha e^{-kh_2} & 0 & -i\alpha(e^{-k(h_2-h_1)}+e^{-2k})/2 & -ikc_2 \end{pmatrix}.$$

Matrix **A** describes the interaction between the two surface waves (the prograde and the retrograde) and the two vorticity waves and its eigenvalues and eigenvectors determine the frequencies, growth rates, and vertical structure of the modes of Eq. (10).

A. Modal instability interpreted in terms of edge wave interaction

In order to gain insight into the modal instabilities arising from the interaction of the edge waves,[14,10] we study following Heifetz and Methven[18] the evolution of the amplitude and phase of each wave separately by writing the complex amplitudes as

$$[q_0(t),\zeta(t),q_1(t),q_2(t)] = [Q_0(t)e^{i\epsilon_0(t)},Z(t)e^{\epsilon_\zeta t},Q_1(t)e^{i\epsilon_1(t)},Q_2(t)e^{i\epsilon_2(t)}]$$

and taking the real and imaginary parts separately to obtain the following equations for the amplitude of the edge waves:

$$\frac{dQ_0}{dt} = -\frac{kZ}{F^2}\sin\epsilon_{\zeta 0}, \tag{16}$$

$$\frac{dZ}{dt} = Q_0\sin\epsilon_{\zeta 0} - \frac{\sigma_{10}}{\alpha}Q_1\sin(\epsilon_{10}-\epsilon_{\zeta 0}) - \frac{\sigma_{20}}{\alpha}Q_2\sin(\epsilon_{20}-\epsilon_{\zeta 0}), \tag{17}$$

$$\frac{dQ_1}{dt} = \sigma_{10}Q_0\sin\epsilon_{10} + \sigma_{12}Q_2\sin\epsilon_{12}, \tag{18}$$

$$\frac{dQ_2}{dt} = -\sigma_{20}Q_0\sin\epsilon_{20} + \sigma_{12}Q_1\sin\epsilon_{12}, \tag{19}$$

where $\epsilon_{\zeta 0}=\epsilon_\zeta-\epsilon_0$, $\epsilon_{10}=\epsilon_1-\epsilon_0$, $\epsilon_{20}=\epsilon_2-\epsilon_0$, and $\epsilon_{12}=\epsilon_1-\epsilon_2$ are the phase differences between the edge waves, and the coefficients,

$$\sigma_{12} = \alpha(e^{-k(h_2-h_1)}+e^{-k(h_1+h_2)})/2,$$

$$\sigma_{10} = \alpha e^{-kh_1}, \quad \sigma_{20} = \alpha e^{-kh_2},$$

indicate the strength of interaction between the edge waves. Equations (16)–(19) show that each wave's amplitude can only grow through interaction with the other two, with the interaction strength depending on two factors: the strength of the flow induced by the other two waves on each wave's interface which is proportional to σ_{ij} $(i,j=0,1,2)$ and falls exponentially with the distance between the interfaces and the phase difference between the waves. The relative phases of the edge waves evolve according to the equations

$$\frac{d\epsilon_{\zeta 0}}{dt} = \frac{F^2Q_0^2-kZ^2}{ZQ_0F^2}\cos\epsilon_{\zeta 0} + \frac{\sigma_{10}Q_1}{\alpha Z}\cos(\epsilon_{10}-\epsilon_{\zeta 0}) + \frac{\sigma_{20}Q_2}{\alpha Z}\cos(\epsilon_{20}-\epsilon_{\zeta 0}), \tag{20}$$

$$\frac{d\epsilon_{10}}{dt} = k(1-c_1) - \frac{kZ}{Q_0F^2}\cos\epsilon_{\zeta 0} + \frac{Q_0}{Q_1}\sigma_{10}\cos\epsilon_{10} + \frac{Q_2}{Q_1}\sigma_{12}\cos\epsilon_{12}, \tag{21}$$

$$\frac{d\epsilon_{20}}{dt} = k(1-c_2) - \frac{kZ}{Q_0F^2}\cos\epsilon_{\zeta 0} - \frac{Q_0}{Q_2}\sigma_{20}\cos\epsilon_{20} - \frac{Q_1}{Q_2}\sigma_{12}\cos\epsilon_{12}, \tag{22}$$

$$\frac{d\epsilon_{12}}{dt} = -k(c_1-c_2) + \sigma_{10}\frac{Q_0}{Q_1}\cos\epsilon_{10} + \sigma_{20}\frac{Q_0}{Q_2}\cos\epsilon_{20} + \sigma_{12}\frac{Q_1^2+Q_2^2}{Q_1Q_2}\cos\epsilon_{12}. \tag{23}$$

The fixed points of Eqs. (20)–(23) determine the phase locked configuration of the modal solutions. Note that when the edge waves are exactly in phase or out of phase ($\epsilon_{ij}=0,\pi$), the amplitude tendency is zero and when the phase difference is $\epsilon_{ij}=\pi/2$, the amplitude tendency is maximized while their phase difference tendency is determined only by the differences in the phase speeds of the waves as seen in Eq. (23).

Longuet-Higgins[8] obtained the stability properties of this flow for various values of h_1 and F and found two branches of instability. In order to analyze modal instability in terms of edge wave interactions, it is instructive to consider first two separate limits that isolate the edge wave interactions underlying the dynamics of the two corresponding branches of instability.

1. The small Froude number limit

Consider first the limit of small Froude number $F \ll 1$ in which limit the surface acts as a rigid lid. In steady state, the free surface displacement in this limit is $ZO(F)$ and the surface wave is such that the vertical velocity at the surface is small $[v(y=0)=i(q_0+q_1e^{-kh_1}+q_2e^{-kh_2})O(F^2)]$. As a result $q_0=-q_1e^{-kh_1}-q_2e^{-kh_2}+O(F^2)$ and Eqs. (18), (19), and (23) can be approximated in this case by

$$\frac{dQ_1}{dt} \approx \tilde{\sigma}_{12}Q_2\sin\epsilon_{12}, \tag{24}$$

$$\frac{dQ_2}{dt} \approx \tilde{\sigma}_{12}Q_1\sin\epsilon_{12}, \tag{25}$$

$$\frac{d\epsilon_{12}}{dt} \approx -k(\tilde{c}_1-\tilde{c}_2) + \tilde{\sigma}_{12}\frac{Q_1^2+Q_2^2}{Q_1Q_2}\cos\epsilon_{12}, \tag{26}$$

where

$$\tilde{c}_i = U_i + (-1)^i\frac{\alpha(1-e^{-2kh_i})}{2k}, \tag{27}$$

where $i=1,2$, and $\tilde{\sigma}_{12}=\alpha(e^{-k(h_2-h_1)}-e^{-k(h_1+h_2)})/2$. The dynamics are therefore described to a very good approximation by the interaction between the two vorticity waves whose

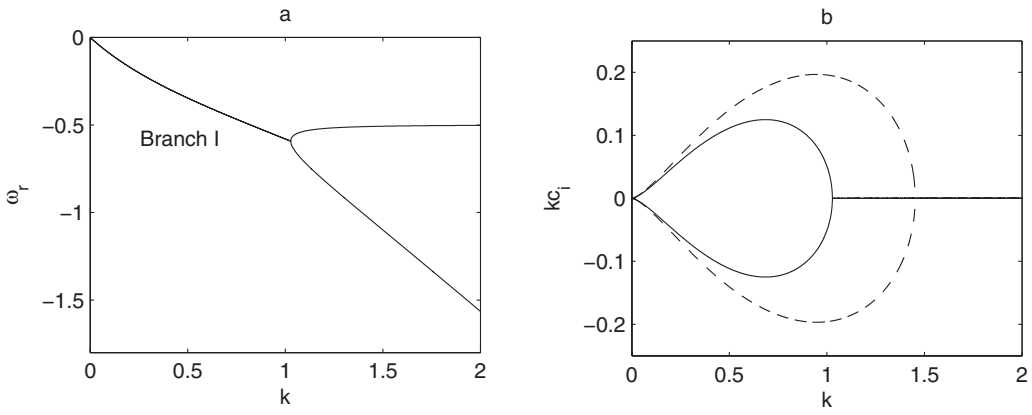

FIG. 2. Dispersion relation for the normal modes of **A** in the limit of small Froude number ($F=0.01$). (a) Real part of frequency ω_r as a function of wavenumber for $h_1=0.5$. The normal modes arising from the interaction of the inner vorticity edge waves are either neutral or unstable and the region of branch I instability is also noted. (b) Growth rate kc_i as a function of wavenumber for $h_1=0.5$ (solid line) and $h_1=0.6$ (dashed line).

phase speeds and interaction strength are modified because of the rigid lid boundary condition.

The closed system (24)–(26) describing the interaction between the vorticity waves was previously studied by Heifetz and Methven[18] (although the phase speeds and the interaction strength are different in that case as Heifetz and Methven[18] considered an unbounded fluid) who found that if the interaction coefficient $\tilde{\sigma}_{12}$ is strong enough to counteract differential wave propagation, that is, if the condition

$$\frac{k(\tilde{c}_1-\tilde{c}_2)}{2\tilde{\sigma}_{12}}<1 \tag{28}$$

is satisfied, Eq. (26) has two fixed points:

$$\epsilon_{12}=\pm\cos^{-1}\frac{k(\tilde{c}_1-\tilde{c}_2)}{2\tilde{\sigma}_{12}},$$

with the edge waves having equal amplitude ($\hat{Q}_1=\hat{Q}_2$). The stable fixed point is in the range $0<\epsilon_{12}<\pi$ and the two edge waves will phase lock in this configuration leading to mutual growth of the vorticity waves, with growth rate

$$\lambda=\tilde{\sigma}_{12}\sin\left(\cos^{-1}\frac{k(\tilde{c}_1-\tilde{c}_2)}{2\tilde{\sigma}_{12}}\right).$$

This phase locked state corresponds to the growing normal mode of branch I instability of Triantafyllou and Dimas.[3] The dispersion relation for the normal modes of the system obtained through eigenanalysis of **A** is shown in Fig. 2 and the configuration of the fastest growing mode is shown in Fig. 3. Amplification occurs as the vertical velocity induced by the lower vorticity wave at the upper interface advects the mean flow vorticity and produces a positive (negative) vorticity tendency just to the right of the positive (negative) upper vorticity anomaly with a similar enhancing vorticity tendency induced by the upper vorticity wave at the lower interface.

For large wavenumbers, differential wave propagation becomes large, whereas the flow induced by each vorticity wave on the other wave's interface that is proportional to $\tilde{\sigma}_{12}$ becomes exponentially small. As a result condition (28) is not satisfied and phase speed matching and resonance are feasible only if the influence of each vorticity wave on the other's propagation rate is maximized which is achieved for $\epsilon_{12}=0,\pi$. In this configuration, the vorticity waves cannot grow and the resulting normal modes are neutrally stable.

For small wavenumbers, the interaction strength is of the same order as the difference in phase speeds and phase locking can occur for waves that are in a growing configuration, with a nevertheless relatively small growth rate. As a result, the maximum growth rate occurs for the wavenumber for which the interplay between the exponential decrease in interaction strength with wavenumber and the requirement of balancing differential propagation to enable phase speed matching yields the optimal mutual amplitude growth. Therefore, for increasing shear the maximum growth rate increases and occurs for larger wavenumbers as shown in Fig. 2 due to the increase in interaction strength $\tilde{\sigma}_{12}$.

2. The limit of no upper layer

If we take the limit of infinitesimally thin upper layer ($h_1=0$), the upper vorticity edge wave vanishes and only the lower vorticity and the surface edge waves interact. By taking the appropriate boundary conditions at the surface,[24] it can be readily shown that the phase speed of the surface waves is modified in this case and is given by

$$\tilde{c}_\pm=1-\frac{\alpha}{2k}\pm\frac{1}{2k}\sqrt{\alpha^2+\frac{4k}{F^2}}. \tag{29}$$

For large wavenumbers or small Froude numbers modification in the surface waves' phase speed is small ($\tilde{c}_\pm\simeq c_\pm$), whereas for small wavenumbers or large Froude numbers $\tilde{c}_\pm\simeq 1-\alpha/k$, and the dispersion relation follows closely that of a Rossby wave (for a thorough discussion of the dynamics of this mixed Rossby-gravity edge wave see Ref. 25).

In this limit, Eqs. (16)–(23) are reduced to

$$\frac{dQ_0}{dt}=-\frac{kZ}{F^2}\sin\epsilon_{\zeta 0}-\sigma_{20}Q_2\sin\epsilon_{20}, \tag{30}$$

$$\frac{dZ}{dt}=Q_0\sin\epsilon_{\zeta 0}-\frac{\sigma_{20}}{\alpha}Q_2\sin(\epsilon_{20}-\epsilon_{\zeta 0}), \tag{31}$$

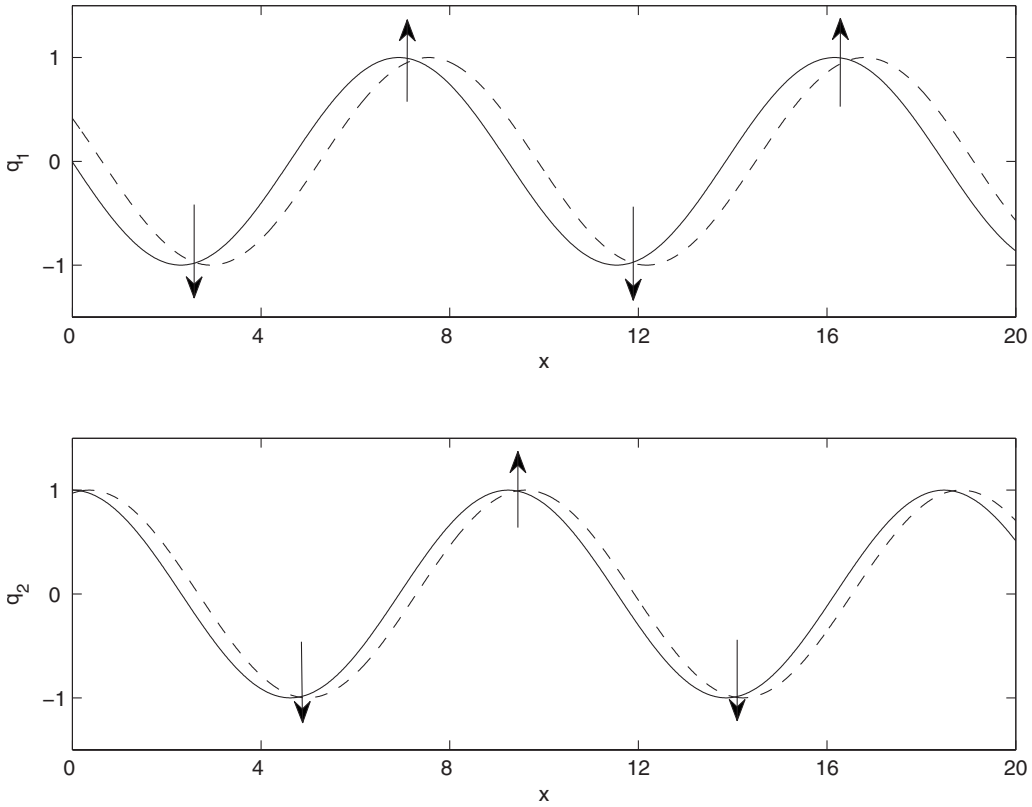

FIG. 3. Illustration of the interaction between the vorticity edge waves for $F=0.01$ and $h_1=0.5$. Vorticity anomalies at $y=-h_1$ (upper panel) and $y=-h_2$ (lower panel) of unit amplitude are shown in the configuration of the most unstable mode ($k=0.68$). The initial anomalies (solid line) would counterpropagate in the absence of interaction with phase speeds given by Eq. (27) to reach the position shown by the dashed line after $t=1$. The arrows show the locations of maximum positive (upward arrow) and minimum negative (downward) vorticity tendencies induced by each wave at $t=0$ on the other wave's interface through advection of the basic state vorticity. This interaction slows down the waves and leads to mutual amplitude growth.

$$\frac{dQ_2}{dt} = -\sigma_{20} Q_0 \sin \epsilon_{20}, \tag{32}$$

$$\frac{d\epsilon_{\zeta 0}}{dt} = -\alpha + \frac{Q_0^2 F^2 - kZ^2}{ZQ_0F^2}\cos \epsilon_{\zeta 0} + \frac{\sigma_{20} Q_2}{\alpha Z}\cos(\epsilon_{20} - \epsilon_{\zeta 0}) - \sigma_{20}\frac{Q_2}{Q_0}\cos \epsilon_{20}, \tag{33}$$

$$\frac{d\epsilon_{20}}{dt} = (k - \alpha - kc_2) - \frac{kZ}{Q_0F^2}\cos \epsilon_{\zeta 0} - \sigma_{20}\frac{Q_0^2 + Q_2^2}{Q_0 Q_2}\cos \epsilon_{20}. \tag{34}$$

Following the analysis in the previous section, it can be shown that when the interaction strength between the lower vorticity wave and the retrograde surface wave is large enough to counteract their differential wave propagation, Eqs. (33) and (34) have stable fixed points in the ranges $-\pi < \epsilon_{\zeta 0} < 0$ and $-\pi < \epsilon_{20} < 0$ for which there is mutual growth of the vorticity and the retrograde surface wave amplitude, as Eqs. (30)–(32) indicate. This phase locked state corresponds to the growing normal mode of branch II instability of Triantafyllou and Dimas[3] and the configuration of the fastest growing mode is shown in Fig. 4. The surface wave is amplified as the vertical velocity induced by the lower vorticity wave at the surface alters the vertical displacement of the free surface that in turn enhances the vorticity of the retrograde surface wave when their relative phase difference lies between 0 and $-\pi$. Similarly the surface wave induces a vertical velocity at the lower interface of vorticity discontinuity, advecting the mean flow vorticity and producing a positive (negative) vorticity tendency just to the left of the positive (negative) vorticity anomaly, leading to growth of the lower vorticity wave.

We can see in Fig. 5, showing the growth rate for these vorticity-gravity wave modes, that unstable normal modes exist for only a limited range of wavenumbers. For both small and large horizontal scales, the difference in phase speeds $\tilde{c}_{\pm} - c_2$ is large, while the interaction strength σ_{20} is exponentially small. Therefore, phase locking is only possible for $\epsilon_{\zeta 0}, \epsilon_{20} = 0, \pi$, for which the influence of each edge wave on the other's propagation rate is maximized, yielding neutrally stable normal modes. The fast neutral mode arises from the interaction of the fast (prograde) surface wave with the inner (prograde) vorticity wave and its phase speed follows closely $\tilde{c}_+$. The two slow ones arise from the interaction of the slow (retrograde) surface wave with the inner (prograde) vorticity wave. For large wavenumbers their phase speed follows closely $\tilde{c}_-$ and c_2, respectively, while for small wavenumber their dispersion relation has the characteristics of a surface wave and an inner vorticity wave with modified phase speeds.

For increasing Froude numbers, resonance for waves with large wavelengths can occur for $\epsilon_{20} \neq 0, \pi$ because the

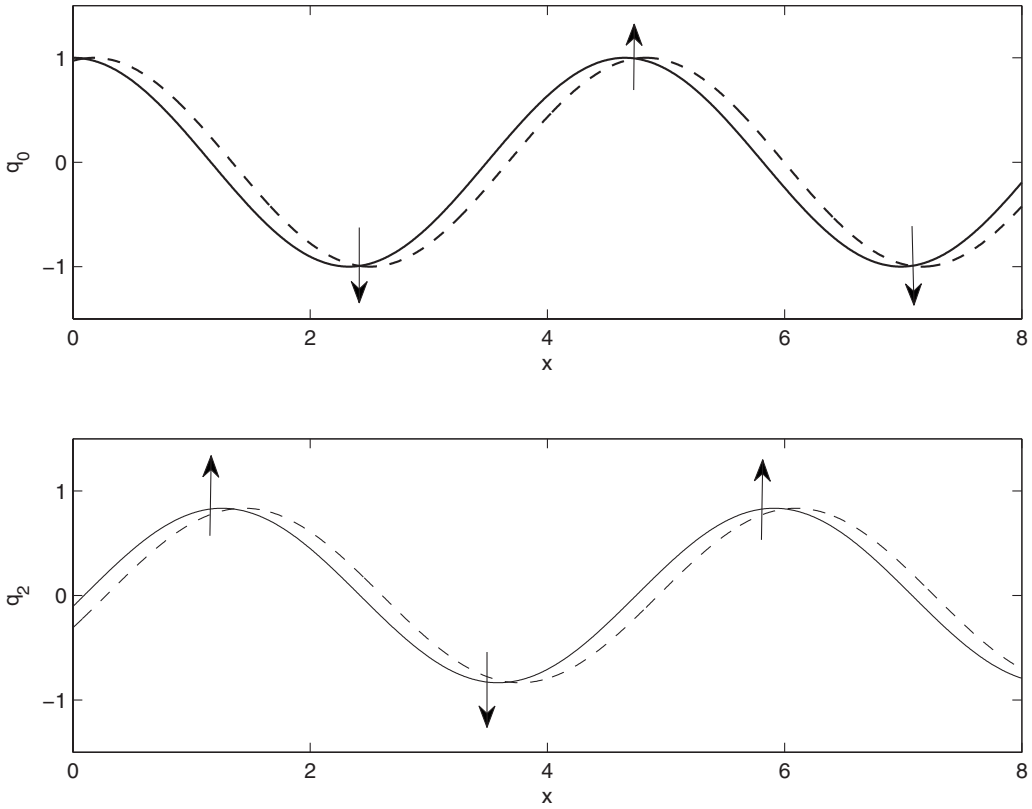

FIG. 4. Illustration of the interaction between the lower vorticity and the surface edge wave for $F=\sqrt{2}$ and $h_1=0$. Vorticity anomalies at $y=0$ (upper panel) and $y=-h_2$ (lower panel) of unit amplitude are shown in the configuration of the most unstable mode ($k=1.35$). The initial anomalies (solid line) would counterpropagate in the absence of interaction with phase speeds given by Eqs. (29) and (15) to reach the position shown by the dashed line after $t=1$. The arrows show the locations of maximum positive (upward arrow) and minimum negative (downward arrow) vorticity tendencies induced by each wave at $t=0$ on the other wave's interface. We also note that the vertical displacement for the surface wave is almost in phase with the vorticity. This interaction slows down the waves and leads to mutual amplitude growth.

intrinsic frequency of the surface wave decreases, resulting in a smaller differential propagation. As a result the range of wavenumbers for which there are exponentially growing modes increases and is shifted toward smaller wavenumbers, as illustrated in Fig. 5. Since for smaller wavenumbers the strength of interaction σ_{20} increases, the maximum growth rate increases as well.

3. Finite Froude number and upper layer depth

A typical example of the dispersion relation for finite Froude number and upper layer depth in which all edge waves interact and both branches of instability are present is shown in Fig. 6, which is similar to Fig. 2 of Longuet-Higgins.[8] The configuration of the fastest growing

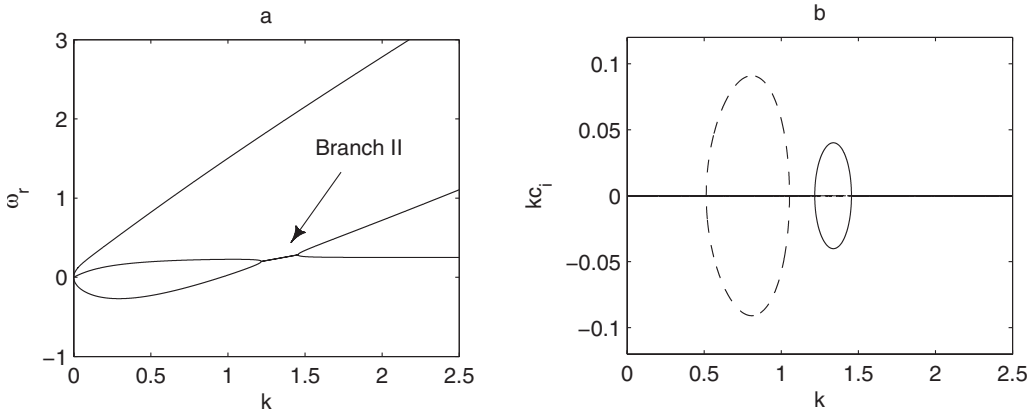

FIG. 5. Dispersion relation for the normal modes of **A** in the limit of infinitesimal upper layer ($h_1=0$). (a) Real part of frequency ω_r as a function of wavenumber for $F=\sqrt{2}$. The fast neutral mode arises from the interaction of the fast (prograde) surface wave with the inner (prograde) vorticity wave. The two slower ones arise from the interaction of the slow (retrograde) gravity wave with the inner (prograde) vorticity wave and can be neutral or unstable. The region of branch II instability is also noted. (b) Growth rate kc_i as a function of wavenumber for $F=\sqrt{2}$ (solid line) and $F=3$ (dashed line).

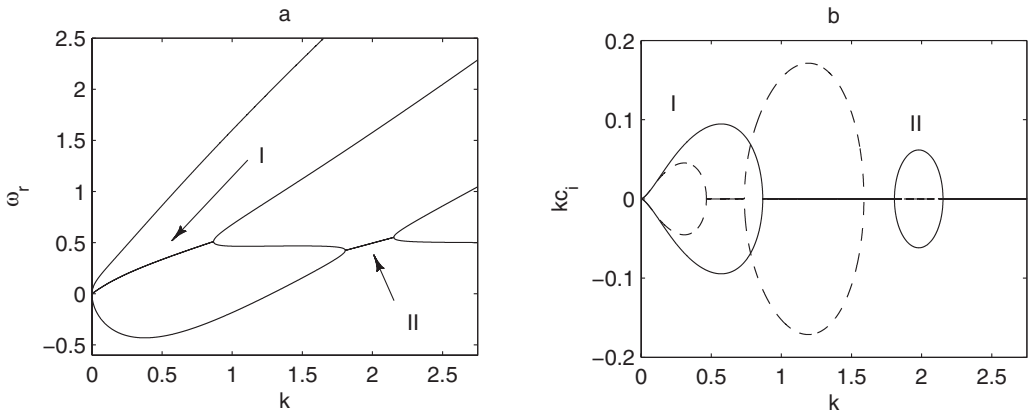

FIG. 6. Dispersion relation for the normal modes of **A** arising from the interaction of the vorticity edge waves with the surface gravity waves. (a) Real part of frequency ω_r as a function of wavenumber for $F=1$. (b) Growth rate kc_i as a function of wavenumber for $F=1$ (solid line) and $F=2$ (dashed line). The upper layer depth is $h_1=0.5$. In both panels the regions of branch I and branch II instabilities are also noted.

branch I instability resulting mainly from the interaction of the two vorticity waves is shown in Fig. 7. Since the strength of the flow induced by the edge waves falls exponentially with the distance between the interfaces, the surface gravity wave affects mainly the upper vorticity wave. The stable fixed point of Eq. (21) for a growing normal mode is in the range $-\pi<\epsilon_{10}<0$ for which the vertical velocity induced by the surface gravity wave at the upper vorticity interface counteracts the vertical velocity induced by the lower vorticity wave, reducing the positive (negative) vorticity tendency in regions of positive (negative) upper vorticity anomaly. The effect of the surface gravity wave is therefore stabilizing and the growth rate of branch I instability decreases for larger Froude numbers as shown in Fig. 6, in agreement with the findings of Longuet-Higgins.[8] Moreover the surface gravity wave tends to speed up the upper vorticity wave relative to the mean flow at the upper interface, increasing the differential propagation of the two vorticity waves. As a re-

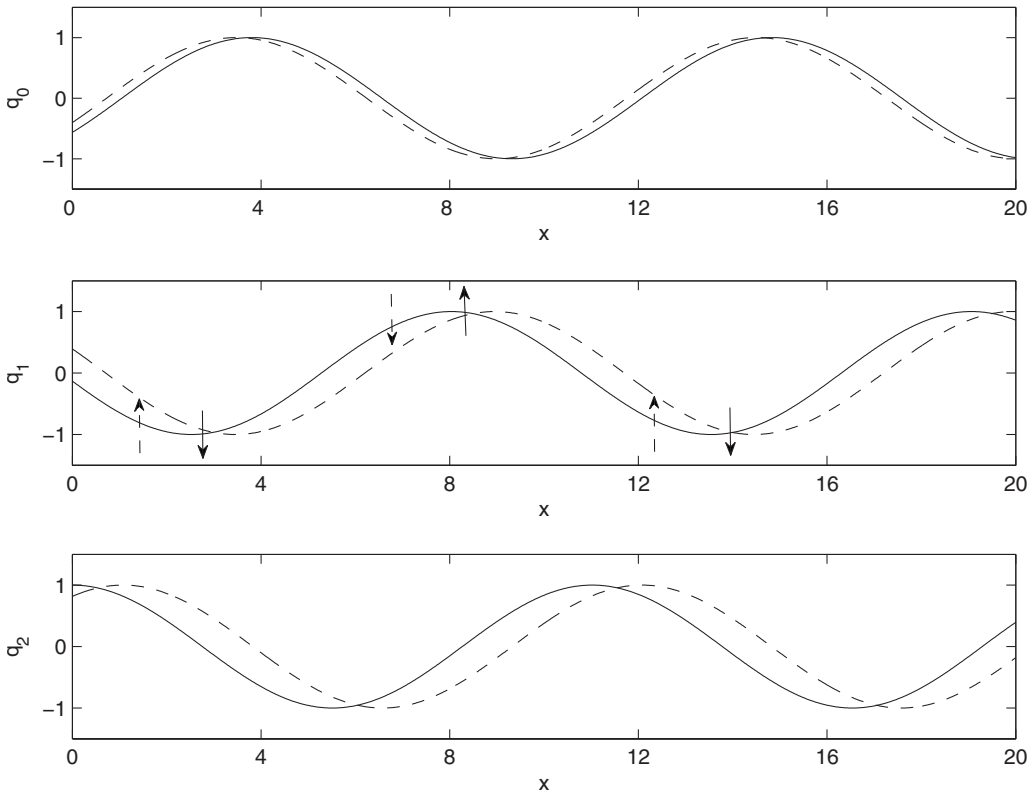

FIG. 7. Illustration of the edge wave interactions for $F=1$ and $h_1=0.5$. Vorticity anomalies at $y=0$ (upper panel), at $y=-h_1$ (middle panel), and at $y=-h_2$ (lower panel) of unit amplitude are shown in the configuration of the most unstable branch I mode ($k=0.57$). The initial vorticity anomalies (solid line) would propagate in the absence of interaction with phase speeds given by Eqs. (14) and (15) to reach the position shown by the dashed line after $t=1$. The arrows show the locations of maximum positive (upward arrow) and minimum negative (downward arrow) vorticity tendencies induced by the lower vorticity wave (solid arrows) and surface gravity wave (dashed arrows) at $t=0$ on the upper vorticity wave's interface ($y=-h_1$) through advection of the basic state vorticity. We also note that the vertical displacement for the surface wave is lagging surface vorticity by almost one-tenth of a wavelength.

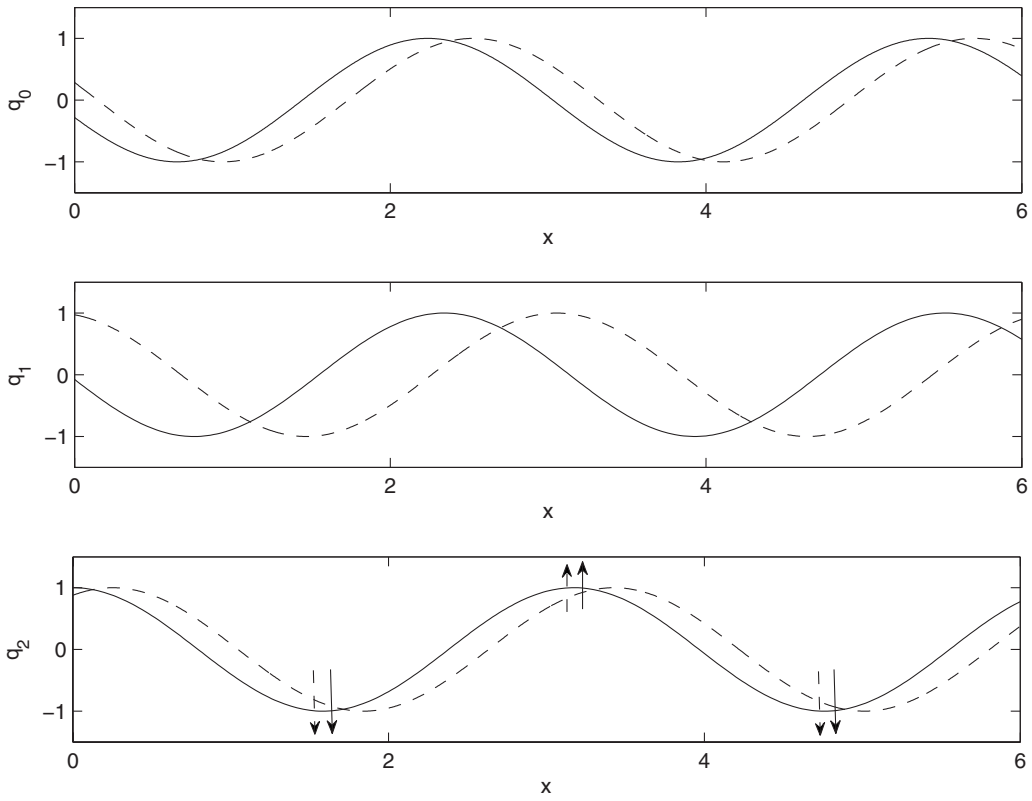

FIG. 8. The same as in Fig. 7 but in the configuration of the most unstable branch II mode ($k=1.98$). The arrows show the locations of maximum positive (upward arrow) and minimum negative (downward arrow) vorticity tendencies induced by the upper vorticity wave (solid arrows) and surface gravity wave (dashed arrows) at $t=0$ on the lower vorticity wave's interface ($y=-h_2$) through advection of the basic state vorticity. We also note that the vertical displacement for the surface wave is almost in phase with the vorticity.

sult, phase speed matching for moderate wavenumbers occurs only for in phase or out of phase edge waves and the cut-off wavenumber is reduced for larger Froude numbers as shown in Fig. 6.

On the other hand in the growing phase locked configuration of branch II instability, the upper vorticity wave enhances the interaction between the lower vorticity and the retrograde surface gravity wave as illustrated in Fig. 8, where the configuration of the fastest growing branch II instability is shown and increases the growth rate of branch II instability. Therefore, as noted by Longuet-Higgins,[8] for small Froude numbers, low wavenumbers of branch I instability dominate the growth, while for large Froude numbers smaller scales of branch II instability dominate, with the two branches having comparable growth rates for moderate Froude numbers. We finally note that increasing shear amplifies the destabilizing effect of the upper vorticity wave and for large enough shear branch I and branch II instabilities merge.

III. DETERMINATION OF THE OPTIMAL GROWTH

In realistic geophysical and laboratory flows, perturbation growth occurs over a finite time interval due to disruption by turbulence or changes in the mean flow. It is therefore of interest to find the initial conditions yielding the largest instantaneous energy growth or the largest energy growth over a specified time interval T_{opt}. In practice T_{opt} is the time scale over which growth is limited and is typically of the order of a few advective time units. We will first address energy growth by taking into account only the discrete spectrum, whose dynamics is governed by the edge wave interactions considered in the previous section.

A. Nonmodal transient growth of the edge waves

It can be readily shown that the nondimensional, zonally averaged perturbation energy is

$$E = \frac{1}{2}\int_{-\infty}^{0} (\overline{u^2+v^2})dy + \frac{1}{2F^2}\overline{\zeta^2}$$
$$= \frac{1}{4}\int_{-\infty}^{0} (|\partial_y\psi|^2 + k^2|\psi|^2)dy + \frac{1}{4F^2}|\zeta|^2, \tag{35}$$

where the overbar denotes a zonal average. If the perturbation field comprises only of the edge waves, perturbation energy (35) is given by

$$E = \mathbf{x}^{\dagger}\mathbf{M}\mathbf{x} = \mathbf{y}^{\dagger}\mathbf{y},$$

where $\dagger$ denotes the Hermitian transpose, $\mathbf{x}=[q_0(t), \zeta(t), q_1(t), q_2(t)]^T$ is the state vector,

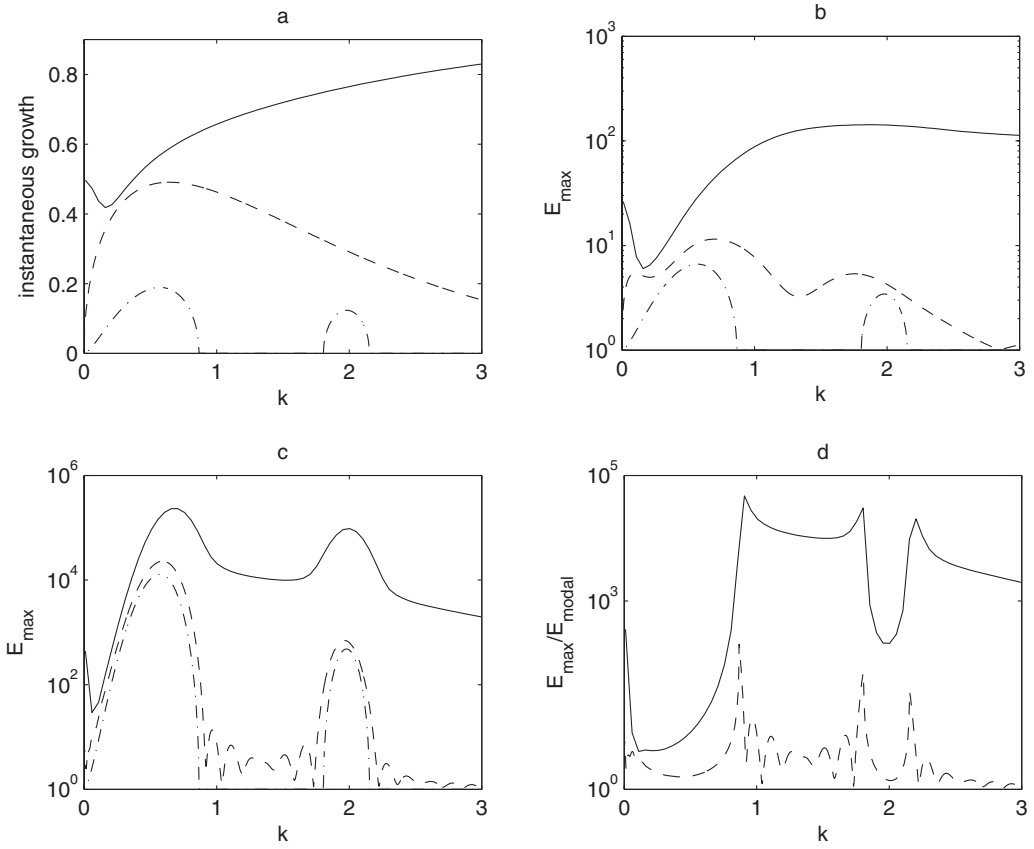

FIG. 9. (a) Optimal instantaneous energy growth for the edge waves (dashed line), for the unstable normal mode (dashed-dotted line), and for the complete spectrum solution (solid line). (b) Optimal energy growth as a function of wavenumber k for a perturbation projecting on the discrete spectrum (dashed line) and on the complete spectrum (solid line). The corresponding growth of the unstable normal mode (dashed-dotted line) is also shown. The optimization time is $T_{\text{opt}}=10$. (c) The same as in (b) but for optimization time $T_{\text{opt}}=50$. (d) Optimal energy growth normalized by the corresponding growth of the unstable mode as a function of wavenumber for a perturbation projecting on the discrete spectrum (dashed line) and on the full spectrum (solid line). The optimization time is $T_{\text{opt}}=50$. In all panels $F=1$ and $h_1=0.5$.

$$\mathbf{M}=\frac{1}{4k}\begin{pmatrix} 1 & 0 & \sigma_{10}/\alpha & \sigma_{20}/\alpha \\ 0 & k/F^2 & 0 & 0 \\ \sigma_{10}/\alpha & 0 & (1+e^{-2kh_1})/2 & \sigma_{12}/\alpha \\ \sigma_{20}/\alpha & 0 & \sigma_{12}/\alpha & (1+e^{-2kh_2})/2 \end{pmatrix}$$

is the energy metric matrix, and $\mathbf{y}=\mathbf{M}^{1/2}\mathbf{x}$ is the state vector in transformed coordinates for which the energy is given by the Euclidean norm of $\mathbf{y}$. The governing equation for $\mathbf{y}$ is

$$\frac{d\mathbf{y}}{dt}=\mathbf{D}\mathbf{y}, \tag{36}$$

where $\mathbf{D}=\mathbf{M}^{1/2}\mathbf{A}\mathbf{M}^{-1/2}$. The solution of Eq. (36) is given by $\mathbf{y}(t)=e^{\mathbf{D}t}\mathbf{y}(0)$, where $\mathbf{y}(0)$ is the initial state and $e^{\mathbf{D}t}$ is the finite time propagator mapping the initial perturbation to its state at time t.

For a given zonal wavenumber k, singular value decomposition of the propagator $e^{\mathbf{D}t}=\mathbf{U}\boldsymbol{\Sigma}\mathbf{V}^{\dagger}$, where $\mathbf{U}$ and $\mathbf{V}$ are unitary matrices and Σ is a diagonal matrix with positive elements ordered by growth, identifies the optimal perturbation $\mathbf{y}_{\text{opt}}$ as the first column of $\mathbf{V}$.[23] The square of the corresponding singular value σ is the largest energy growth $E_{\max}(T_{\text{opt}})$ that can be achieved over the specified time interval T_{opt} by any initial plane wave of unit energy with wavenumber k. The maximum instantaneous growth rate is readily obtained by taking the limit $T_{\text{opt}}\to 0$, in which case the analysis is reduced to finding the leading eigenvalue and the corresponding eigenvector of $(1/2)(\mathbf{D}+\mathbf{D}^{\dagger})$.[23]

The maximum instantaneous growth rate as a function of wavenumber for Froude number $F=1$ and $h_1=0.5$ is shown in Fig. 9(a) along with the corresponding growth rate for the most unstable normal mode of $\mathbf{A}$. Perturbation energy grows instantaneously even for the range of wavenumbers k for which there are no unstable modes, as the amplitudes of the edge waves can grow transiently in the time interval before phase locking regardless of the steady state phase difference between the edge waves that determines whether the resulting normal mode grows exponentially or not.

The optimal energy growth $E_{\max}$ achieved at $T_{\text{opt}}=10$ and $T_{\text{opt}}=50$ as a function of wavenumber is shown in Figs. 9(b) and 9(c), respectively. For small optimizing times, the optimal growth has two peaks in the branch I and II instability regions, respectively, while there is also comparable growth for the stable region of wavenumbers in between the two branches. For larger optimizing times, most of the energy amplification observed in the unstable regions is attributed to the growth of the unstable normal modes because phase locking occurs within about 15 advective time units. In this case, the optimal initial condition leads to a rapid energy

amplification in the time interval before phase locking and to the excitation of the normal mode with a finite amplitude. For the most unstable wavenumber in both branches of instability, this results in an overall energy growth that is about two times the corresponding growth attained by initially perturbing the flow with the unstable normal mode, as can be seen in Fig. 9(d). In the vicinity of the stability boundaries, optimal growth is up to two orders of magnitude larger than the normal mode growth that is either very low or zero, whereas for wavenumbers far within the stable regions, optimal growth diminishes as well with only about a doubling of the initial energy.

In summary, perturbation energy growth occurs even for wavenumbers for which exponentially growing modes are absent and is significant for early optimization times. For larger optimization times normal mode instability dominates if we only take into account the discrete spectrum, that is, the edge wave dynamics. The configuration of the optimal edge wave initial condition facilitates non-normal edge wave interactions in the time interval before phase locking, leading to the excitation of the normal mode with a modest amplitude.

B. The role of the continuous spectrum in optimal growth

In addition to the discrete spectrum studied in previous sections, Eq. (10) has a continuous spectrum of singular modes that are neutral. Since these modes are nonorthogonal, they can cooperate to produce transient growth. This can be easily seen by considering an unbounded constant shear flow $U(y)=\alpha y$ without a free surface. In this case Eq. (10) has only a continuous spectrum of singular neutral modes[19] and the solution of Eq. (10) consisting of the integral over the singular modes can be also insightfully written as the integral over the Orr plane waves[22] with time dependent vertical wavenumber $l-\alpha kt$:

$$\psi_{\mathrm{Orr}}(y,t)=\frac{Ae^{i(l-\alpha kt)y}}{k^2+(l-\alpha kt)^2},$$

each yielding an energy density growth:

$$E_{\mathrm{Orr}}=\frac{k^2+l^2}{k^2+(l-\alpha kt)^2}.$$

The energy density of the plane wave with wavenumbers (k,l) at $t=0$ will reach maximum energy $1+(l/k)^2$ at $t=l/k\alpha$. As these plane waves conserve vorticity, the energy amplification is attributed to kinematic deformation of vorticity by the shear flow leading to transient growth of the cross-stream and streamwise velocity fields for waves with constant phase lines oriented against the mean shear. This is the mechanism of growth in two dimensional shear discussed by Orr[26] and we will refer to it as the Orr mechanism. Since it can lead to a large transient growth of perturbations with phase lines initially oriented almost horizontally $(l/k\gg 1)$, the continuous spectrum has to be taken into account to properly address the stability of the flow at finite time. To obtain the evolution of perturbations projecting on the full spectrum, we use the mean velocity profile

$$U(y)=\begin{cases}1 & \text{for } -h_1+\eta<y\le 0,\\ 1-2\eta/(h_2-h_1)f[(-y-h_1+\eta)/(2\eta)] & \text{for } -h_1-\eta<y\le -h_1+\eta,\\ (y+h_2)/(h_2-h_1) & \text{for } -h_2+\eta<y\le -h_1-\eta,\\ 2\eta/(h_2-h_1)f[(y+h_2+\eta)/(2\eta)] & \text{for } -h_2-\eta<y\le -h_2+\eta,\\ 0 & \text{for } y\le -h_2-\eta,\end{cases}$$

with

$$f(x)=\begin{cases}\frac{2}{3}x^3, & 0\le x<\frac{1}{2},\\ -\frac{2}{3}x^3+2x^2-x+\frac{1}{6}, & \frac{1}{2}\le x<1.\end{cases}$$

It differs from the profile given in Eq. (1) only in that the corners at the edges of the shear region have been smoothed out. We then discretize Eqs. (10) and (35) at points $(y_1,y_2,\ldots,y_N)$ to obtain the matrix equations

$$\frac{d\mathbf{x}_c}{dt}=\mathbf{A}_c\mathbf{x}_c$$

and $E=\mathbf{x}_c^{\dagger}\mathbf{M}_c\mathbf{x}_c$, where $\mathbf{x}_c=[\zeta(t),\psi(y_1,t),\psi(y_2,t),\ldots,\psi(y_N,t)]^T$ is the state vector, $\mathbf{A}_c$ is the dynamical operator, and $\mathbf{M}_c$ is the corresponding energy metric which approximates Eq. (35) with the bilinear form $\mathbf{x}_c^{\dagger}\mathbf{M}_c\mathbf{x}_c$. For the reported calculations we used $N=600$ grid points in a domain of depth $H=8$.

Proceeding as in the previous section, eigenanalysis of $(1/2)(\mathbf{D}_c+\mathbf{D}_c^{\dagger})$, where $\mathbf{D}_c=\mathbf{M}_c^{1/2}\mathbf{A}\mathbf{M}_c^{-1/2}$, reveals the initial perturbation leading to the maximum instantaneous growth, while singular value decomposition of the propagator $e^{\mathbf{D}_c T_{\mathrm{opt}}}$ identifies the initial perturbation of unit energy leading to the largest energy amplification over the specified time interval T_{opt}.

The maximum instantaneous growth and the optimal energy growth $E_{\max}$ achieved at $T_{\mathrm{opt}}=10$ and $T_{\mathrm{opt}}=50$ are shown in Figs. 9(a) and 9(b), respectively. We can see that for small optimizing times optimal energy growth is almost constant for perturbations with wavenumbers $1.5<k<3$, even though only perturbations with wavenumbers close to $k=2$ are exponentially growing. Moreover, comparison of

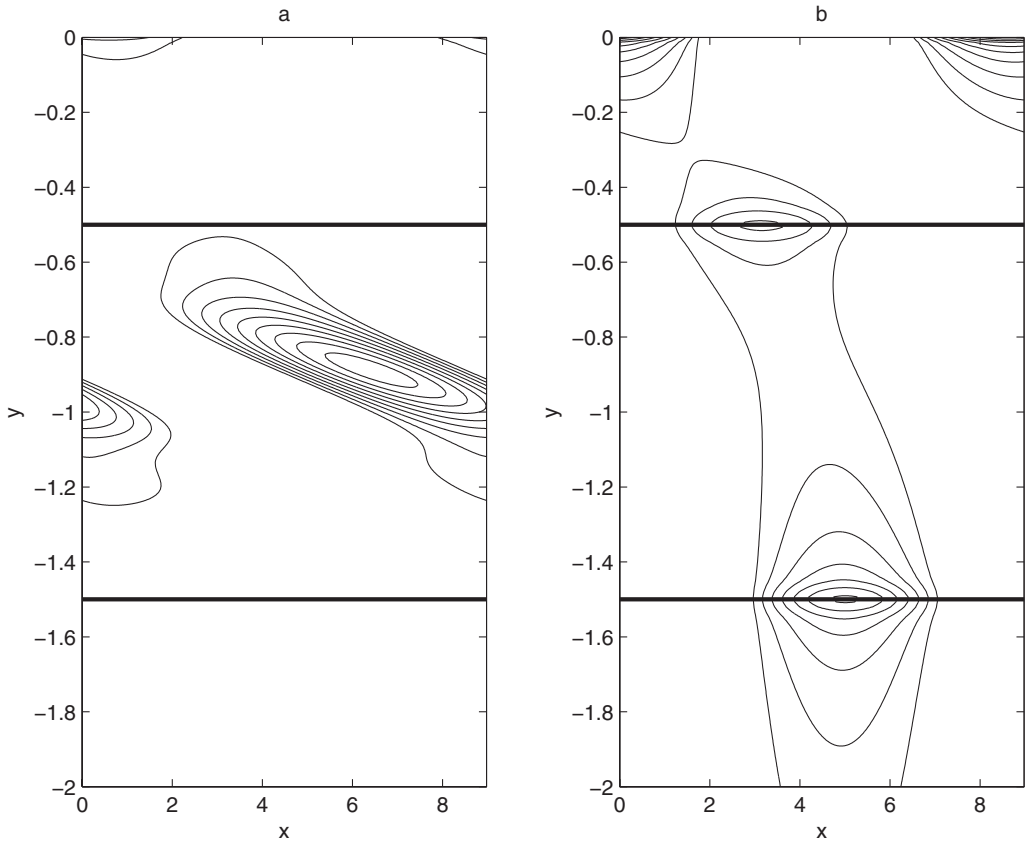

FIG. 10. (a) Streamfunction of the optimal perturbation for optimizing time $T_{opt}=50$. (b) Streamfunction of the unstable normal mode. In both panels, the zonal wavenumber is $k=0.7$, $F=1$, $h_1=0.5$, and the thick lines indicate the boundaries of the shear layer extending from $y=-0.5$ to $y=-1.5$.

the optimal growth with the corresponding exponential growth and the non-normal energy growth due to edge wave dynamics shows that both the normal mode analysis and the edge wave dynamics fail to predict the wavelength of the fastest growing perturbation for early times.

For larger optimizing times, there is significant energy growth peaking in the region of branch I instability with a secondary peak in the region of branch II instability. However, even in this case in which most of the growth is attributed to the exponentially growing normal mode, maximum energy growth occurs for $k=0.7$, while the fastest exponentially growing perturbation has $k=0.57$. For the most unstable wavenumbers of branch I ($k=0.57$) and branch II ($k=1.95$), optimal growth is larger than the corresponding growth of the unstable normal mode by factors of $O(10)$ and $O(200)$, respectively, and about 5 times and 100 times larger than the growth due to non-normal edge wave interactions, respectively. As discussed previously, this excess growth is attributed to the energy amplification occurring in the time interval before phase locking and is caused by the increased excitation of the unstable normal mode shown in Fig. 10 by the initial perturbation projecting on the continuous spectrum. The optimal initial perturbation shown in Fig. 10 has the form of an Orr wave with phase lines tilted against the shear and reveals that the Orr mechanism underlies the transient growth occurring before phase locking.

In the stable regime, the energy growth is about an order of magnitude less than the growth of unstable horizontal scales but is still significantly large and about four orders of magnitude larger than the corresponding growth of perturbations projecting only on the discrete spectrum as can be seen in Fig. 9(d). The initial tilt of the optimal perturbation shown in Fig. 11 is such that the Orr wave assumes a cross-stream orientation ($l/\alpha k - t = 0$) at a time $t \leq T_{opt}$, utilizing the Orr mechanism for transient growth and exciting at high amplitude the four neutral modes. This excitation process leads to the energy vacillation shown in Fig. 11.

IV. CONCLUSIONS

Modal and nonmodal growths of perturbations in the shear flow with a free surface considered by Longuet-Higgins[8] were investigated. The fundamental physical mechanisms underlying the emerging normal mode instabilities have been explored in terms of the interactions between vorticity waves propagating at the two interfaces of vorticity gradient discontinuity and surface gravity waves propagating at the interface of density discontinuity. The vorticity and surface gravity edge waves interact by inducing velocities at the other waves' interfaces that modify the other waves' amplitudes and phase speeds. The efficiency of this interaction was found to be determined by the strength of the induced flow falling exponentially with the horizontal wavelength and by the relative phase difference between the waves. The resulting phase locked configuration corresponds to the normal modes of the shear flow that can be either growing/

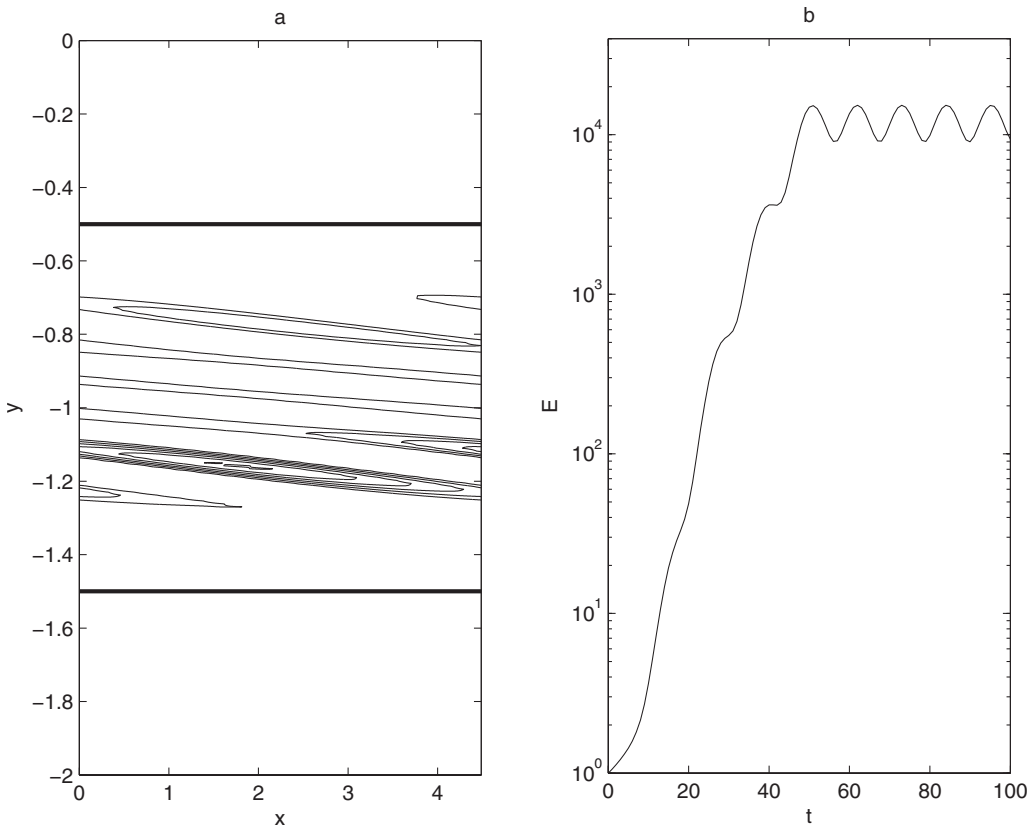

FIG. 11. (a) Streamfunction of the optimal perturbation for optimizing time $T_{opt}=50$. The zonal wavenumber is $k=1.4$ and the thick lines indicate the boundaries of the shear layer extending from $y=-0.5$ to $y=-1.5$. (b) Energy evolution of the optimal perturbation. The Froude number is $F=1$ and $h_1=0.5$.

decaying or neutral depending on the amplitude tendency of the edge waves in the phase locked configuration.

In the limit of small Froude number in which the free surface displacement is infinitesimally small, the dominant interaction is the one between the two counterpropagating vorticity waves. In this case, phase speed modification by the vorticity waves is larger than their differential propagation for large wavelengths, causing the relative phase difference between the vorticity waves in the phase locked state to be in the range between 0 and π. In this configuration the vertical velocity induced by the upper (lower) vorticity wave at the lower (upper) interface advects the mean flow vorticity and produces a vorticity anomaly tendency that reinforces the existing anomaly at the upper (lower) interface. The unstable mode resulting from this interaction corresponds to branch I instability of Triantafyllou and Dimas.[3]

In the limit of no upper layer of constant velocity, only the lower vorticity and the surface waves interact as the upper interface of vorticity gradient discontinuity along with the upper vorticity wave vanishes. For a certain range of wavenumbers the effect of each wave on the propagation rate of the other is strong enough to bring their relative phase difference in the range between $-\pi$ and 0 in the phase locked state. In this configuration there is mutual growth of the vorticity and the retrograde surface wave amplitude, as the vertical velocity induced by the lower vorticity wave at the surface changes the vertical displacement of the free surface that in turn enhances the vorticity of the surface wave, while the surface wave induces a vertical velocity at the lower interface of vorticity discontinuity, advecting the mean flow vorticity and producing a vorticity tendency reinforcing the vorticity anomaly. The resulting normal mode is therefore unstable and corresponds to branch II instability of Triantafyllou and Dimas.[3] For finite Froude number and upper layer depth, the surface gravity wave was found to have a stabilizing effect on branch I instability, while the upper vorticity wave was found to have a destabilizing effect on branch II instability. As a result, for small Froude numbers, large scales of branch I instabilities were found to dominate the exponential growth, while for large Froude numbers, smaller scales of branch II instability have the largest growth rate.

Apart from exponential growth in the phase locked state, the edge waves' amplitudes grow transiently, leading to an algebraic perturbation energy growth at finite time. Calculation of the initial phase and amplitude for each wave yielding the largest energy growth showed that transient energy amplification occurs even for wavenumbers for which exponentially growing modes are absent and is significant for early optimization times. For larger optimization times, perturbations with horizontal scales within branch I and branch II instability regions were found to exhibit the largest transient growth with most of the energy amplification attributed to the growth of the unstable normal modes. In this case, the effect of nonmodal edge wave interactions is to excite the normal mode with modest amplitude due to

their transient growth in the time interval before phase locking.

Finally, nonmodal growth of perturbations taking into account both the discrete and the continuous spectrum of neutral, singular modes of the shear flow was investigated. The energy of vorticity perturbations (Orr waves) initially tilted against the shear amplifies due to kinematic deformation of vorticity by the shear flow. For wavenumbers in the branch I and branch II instability regions, this large amplification leads to excitation of the unstable mode with a large amplitude and to an energy growth that is larger than the corresponding growth of the unstable mode. It was also shown that the horizontal scale of the fastest growing perturbation (in terms of energy norm) is for almost all times different than the scale of the perturbation with the fastest exponential growth.

For wavenumbers in which exponentially growing modes are absent, optimal growth is comparable to the growth obtained by perturbing the flow with the most unstable normal mode. The optimal initial conditions that have the form of an Orr wave with phase lines tilted against the shear lead to the excitation of the four neutral normal modes with a very large amplitude and to an energy vacillation for large times.

In summary, the results of this study lead us to conclude that even though edge wave dynamics are necessary to interpret normal mode instability, nonmodal growth is dominated by the continuous spectrum dynamics and inclusion of the continuous spectrum is necessary to address the stability properties of the flow at finite time.

ACKNOWLEDGMENTS

The authors would like to thank Eyal Heifetz for fruitful discussions.

[1] M. S. Longuet-Higgins, "Shear instability in spilling breakers," Proc. R. Soc. London, Ser. A **446**, 399 (1994).
[2] J. H. Duncan, "Spilling breakers," Annu. Rev. Fluid Mech. **33**, 519 (2001).
[3] G. S. Triantafyllou and A. A. Dimas, "Interaction of two-dimensional separated flows with a free surface at low Froude numbers," Phys. Fluids A **1**, 1813 (1989).
[4] M. E. Stern and Y. A. Adam, "Capillary waves generated by a shear current in water," Mem. Soc. R. Liege **6**, 179 (1973).
[5] K. Itoh, H. Nakamura, H. Kumamaru, and Y. Kukita, "Internal shear mode instabilities on high speed liquid jet," J. Nucl. Sci. Technol. **41**, 802 (2004).
[6] A. G. Voronovich, E. D. Lobanov, and S. A. Rybak, "On the stability of gravitational-capillary waves in the presence of a vertically nonuniform current," Izv. Atmos. Ocean Phys. **16**, 220 (1980).
[7] E. A. Caponi, H. C. Yuen, F. A. Milinazzo, and P. G. Saffman, "Water-wave instability induced by a drift layer," J. Fluid Mech. **207**, 222 (1991).
[8] M. S. Longuet-Higgins, "Instabilities of a horizontal shear flow with a free surface," J. Fluid Mech. **364**, 147 (1998).
[9] L. Engevik, "A note on the instabilities of a horizontal shear flow with a free surface," J. Fluid Mech. **406**, 337 (2000).
[10] F. P. Bretherton, "Baroclinic instability and the short wave cut-off in terms of potential vorticity," Q. J. R. Meteorol. Soc. **92**, 335 (1966).
[11] N. Harnik and E. Heifetz, "Relating over-reflection and wave geometry to the counter propagating Rossby wave perspective: Toward a deeper mechanistic understanding of shear instability," J. Atmos. Sci. **64**, 2238 (2007).
[12] E. Heifetz, C. H. Bishop, and P. Alpert, "Counter-propagating Rossby waves in the barotropic Rayleigh model of shear instability," Q. J. R. Meteorol. Soc. **125**, 2835 (1999).
[13] L. Rayleigh, "On the stability, or instability, of certain fluid motions," Proc. London Math. Soc. **9**, 57 (1880).
[14] G. I. Taylor, "Effect of variation in density on the stability of superposed streams of fluid," Proc. R. Soc. London, Ser. A **132**, 499 (1931).
[15] S. Goldstein, "On the stability of superposed streams of fluid of different densities," Proc. R. Soc. London, Ser. A **132**, 524 (1931).
[16] S. Sakai, "Rossby–Kelvin instability: A new type of ageostrophic instability caused by a resonance between Rossby waves and gravity waves," J. Fluid Mech. **202**, 149 (1989).
[17] P. G. Baines and H. Mitsudera, "On the mechanism of shear flow instabilities," J. Fluid Mech. **276**, 327 (1994).
[18] E. Heifetz and J. Methven, "Relating optimal growth to counterpropagating Rossby waves in shear instability," Phys. Fluids **17**, 064107 (2005).
[19] K. M. Case, "Stability of inviscid plane Couette flow," Phys. Fluids **3**, 143 (1960).
[20] C. C. Lin, "Some mathematical problems in the theory of the stability of parallel flows," J. Fluid Mech. **10**, 430 (1961).
[21] P. G. Drazin and W. H. Reid, *Hydrodynamic Stability* (Cambridge University Press, Cambridge, 1981).
[22] B. F. Farrell, "Optimal excitation of perturbations in viscous shear flow," Phys. Fluids **31**, 2093 (1988).
[23] B. F. Farrell and P. J. Ioannou, "Generalized stability theory. Part I: Autonomous operators," J. Atmos. Sci. **53**, 2025 (1996).
[24] Since $dU/dy|_{y=0} \neq 0$ for $h_1=0$, the appropriate boundary conditions at the surface in this case are $(\partial_t+ik)\zeta=-ik\psi(0,t)$, $(\partial_t+ik)\partial_y\psi|_{y=0}=-ik\zeta/F^2+i\alpha k\psi(0,t)$.
[25] N. Harnik, E. Heifetz, O. M. Umurhan, and F. Lott, "A buoyancy-vorticity wave interaction approach to stratified shear flow," J. Atmos. Sci. **65**, 2615 (2008).
[26] W. M. F. Orr, "The stability or instability of the steady motions of a perfect liquid and of a viscous liquid," Proc. R. Ir. Acad., Sect. A **27**, 9 (1907).